Biofilm 8 (2024) 100235

Contents lists available at ScienceDirect

Biofilm

journal homepage: www.sciencedirect.com/journal/biofilm

Relaxation-weighted MRI analysis of biofilm EPS: Differentiating biopolymers, cells, and water

Matthew R. Willett [a,d,*], Sarah L. Codd [b,d], Joseph D. Seymour [a,d], Catherine M. Kirkland [c,d]

[a] Department of Chemical Engineering, Montana State University, Bozeman, MT, United States
[b] Department of Mechanical & Industrial Engineering, Montana State University, Bozeman, MT, United States
[c] Department of Civil Engineering, Montana State University, Bozeman, MT, United States
[d] Center for Biofilm Engineering, Montana State University, Bozeman, MT, United States

ARTICLE INFO

Keywords:
Biofilm
MRI
EPS
NMR
AGS

ABSTRACT

Biofilms are a highly complex community of microorganisms embedded in a protective extracellular polymeric substance (EPS). Successful biofilm control requires a variety of approaches to better understand the structure-function relationship of the EPS matrix. Magnetic resonance imaging (MRI) is a versatile tool which can measure spatial structure, diffusion, and flow velocities in three dimensions and in situ. It is well-suited to characterize biofilms under natural conditions and at different length scales. MRI contrast is dictated by T_1 and T_2 relaxation times which vary spatially depending on the local chemical and physical environment of the sample. Previous studies have demonstrated that MRI can provide important insights into the internal structure of biofilms, but the contribution of major biofilm components—such as proteins, polysaccharides, and cells—to MRI contrast is not fully understood. This study explores how these components affect contrast in T_1-and T_2-weighted MRI by analyzing artificial biofilms with well-defined properties modeled after aerobic granular sludge (AGS), compact spherical biofilm aggregates used in wastewater treatment. MRI of these biofilm models showed that certain gel-forming polysaccharides are a major source of T_2 contrast, while other polysaccharides show minimal contrast. Proteins were found to reduce T_2 contrast slightly when combined with polysaccharides, while cells had a negligible impact on T_2 but showed T_1 contrast. Patterns observed in the model biofilms served as a reference for examining T_2 and T_1-weighted contrast in the void spaces of two distinct AGS granules, allowing for a qualitative evaluation of the EPS components which may be present. Further insights provided by MRI may help improve understanding of the biofilm matrix and guide how to better manage biofilms in wastewater, clinical, and industrial settings.

1. Introduction

Biofilms, a consortium of bacteria ensconced in a sticky slime, have existed for billions of years. Nonetheless, in 2019, global leaders in biofilm research boldly declared biofilms were suffering from an "identity crisis" [1]. This uncertainty is not related to the contradictory impacts that biofilms have across multiple sectors; many biofilms cause deadly infections and foul equipment, while others can be harnessed for beneficial purposes, such as biological wastewater treatment. Rather, the identity crisis lies with the slime, more technically termed the extracellular polymeric substances (EPS). The microbially-produced EPS consists of a complex mixture of extracellular DNA, proteins, lipids, and polysaccharides, and is crucial for understanding how biofilms operate [2–4]. However, surprisingly little is known about the identity, function, and distribution of individual components inside this complex matrix, leaving questions such as how deadly biofilms resist antimicrobial treatment, or how to optimally grow wastewater biofilms, incompletely understood.

1.1. Magnetic resonance imaging

To increase the scientific community's understanding of biofilm EPS, researchers called for improved extraction processes to isolate and identify individual biomolecular components [1]. However, this

* Corresponding author. Department of Chemical Engineering, Montana State University, Bozeman, MT, United States.
E-mail addresses: matthewwillett@montana.edu (M.R. Willett), scodd@montana.edu (S.L. Codd), jseymour@montana.edu (J.D. Seymour), catherine.kirkland@montana.edu (C.M. Kirkland).

https://doi.org/10.1016/j.bioflm.2024.100235
Received 18 June 2024; Received in revised form 4 October 2024; Accepted 24 October 2024
Available online 24 October 2024

approach is prone to bias, as different solubilization methods can alter the EPS composition. Therefore, imaging tools are integral to confirm the identity of the EPS as well as to observe how EPS components are spatially distributed throughout the biofilm matrix. Viable approaches include confocal laser scanning microscopy (CLSM), Fourier transform infrared (FTIR) imaging, Raman spectroscopic imaging, scanning transmission X-ray (STXR) microscopy, and mass spectrometry imaging (MSI) [1]. Since this 2019 call for action, advances in the aforementioned methods have led to many breakthroughs in EPS characterization [5]. Noninvasive, label-free magnetic resonance imaging (MRI) complements these techniques by studying the structure and function relationship of biofilm EPS components without being limited by biofilm size and thickness.

MRI is an imaging technique based on the nuclear magnetic resonance (NMR) principle of spin, a quantum mechanical property describing nuclear spin states of atoms such as ^{1}H, ^{13}C, and ^{19}F [6,7]. An NMR magnet supplies an external magnetic field ($\mathbf{B_0}$) which causes a slight majority of spins to align their magnetic moments together and generate a small net magnetization. The spins also precess at the Larmor frequency proportional to the strength of the external magnetic field. After being excited by a radiofrequency pulse also at the Larmor frequency, spins return to equilibrium in a process termed relaxation, during which signal is collected. Due to their high percentage of water (>95 %), biofilms are visualized by exciting ^{1}H nuclei. Images in 1-, 2- or 3-dimensions are created by using magnetic field gradients to localize spin signal [8]. MRI has no depth limitation on biofilm scales and images can be acquired in any spatial orientation by applying slice selection gradients. Moreover, image contrast arises naturally, depending on proton (spin) density, molecular diffusion, chemical shift, and relaxation phenomena. Proton density imaging does not supply strong contrast in biofilm imaging, since water in the hydrated EPS dominates over much smaller populations from intracellular water and protons from EPS macromolecules [8,9]. Diffusion-weighted imaging detects changes in random spin motion, providing contrast between regions where translational motion is restricted such as pores, channels, and intracellular water [10]. Chemical shift arises from changes in the magnetic field experienced by spins on a molecule due to its electron cloud and serves as the basis for magnetic resonance spectroscopy (MRS) in determining the chemical structure and composition of a molecule. Different molecules have different chemical shifts, which can be used as a contrast in MRI, *i.e.*, magnetic resonance spectroscopic imaging (MRSI), to create spatial concentration profiles of specific biofilm molecules [6,11,12,13].

However, the predominant NMR method to characterize biofilms is relaxation-weighted imaging [9,14]. Relaxation occurs due to dipolar spin interactions, which create local variations in the magnetic field that fluctuate due to random Brownian motion. Fluctuations at the Larmor frequency induce spin energy level transitions which lead to the return of the spins to equilibrium, a process termed T_1 relaxation [6,11]. Spins which experience varying local magnetic fields due to dipolar coupling will precess at different frequencies and lose phase coherence, leading to a decay of the magnetization signal, a process termed T_2 relaxation [6,11]. When this decay also includes contributions from static field inhomogeneities, it is termed T_2^* relaxation. The *structure* of a biofilm can influence relaxation rates by limiting the rotational mobility of protons. This restriction occurs in various biofilm components such as the EPS matrix and cell clusters [4]. The *chemical environment* of a biofilm also affects relaxation, through mechanisms such as chemical exchange between protons in water and functional groups on large EPS molecules [15,16]. Also included in this category are susceptibility artifacts present in the biofilm matrix, such as accumulated minerals or other paramagnetic ions, which will influence T_2^*-contrast. Ultimately, it is the complex chemical and physical environment of the biofilm which leads to a divergence of spin T_1, T_2, and T_2^* relaxation times. Parameters in MRI experiments can be adjusted to either emphasize T_1-, T_2-, or T_2^*-relaxation contrast, forming images which can readily differentiate between bulk water and biofilm EPS.

1.2. Characterization of biofilm EPS using MRI

The extent to which MRI can distinguish between individual EPS components has not been fully established. Diffusion-weighted MRI has been used to characterize biofilm heterogeneities to varying degrees of success. Wieland et al. made diffusion maps through a phototrophic biofilm, observing a decrease in diffusivity in zones attributed to high density of cells and EPS [17]. However, in another study, little variation in diffusion coefficients was observed, despite the complex internal structure of the biofilm [18]. Chemical shift methods have the greatest potential to clearly contrast different EPS components. Preliminary work using techniques such as chemical shift selective (CHESS) and chemical exchange saturation transfer (CEST) [6] imaging to target biofilm molecules with specific chemical shifts or exchangeable protons, respectively, is promising [19]. However, there are well-known challenges using MRS for carbohydrate characterization [20] and MRSI has been primarily used to visualize and monitor the distribution of metabolites in different biofilm regions to enhance understanding of biofilm growth dynamics [12,13]. Hoskins et al. first used MRI to visualize biofilms in porous media using relaxation contrast techniques [21]. However, in this and many subsequent studies, relaxation-weighted MRI has largely been used to confirm the presence of a biofilm and broadly characterize its morphology [8]. Kirkland et al. considered specific sources of contrast across T_1-and T_2-weighted images of heterogeneous aerobic granular sludge (AGS) biofilms used for wastewater treatment [22]. It was suggested that lighter pockets in T_2 maps could be from void spaces, darker regions from more tightly crosslinked EPS, and the darkest regions at the center from solid inclusions.

Despite the prevalence of relaxation-weighted MRI to study biofilms, research is needed to clarify the relative contribution of major biofilm and EPS components to MRI contrast. Biofilm constituents all play unique roles and have distinct relaxation behavior. Polysaccharides, particularly gel-forming polysaccharides, often provide structure to biofilms [2,3] and may strongly affect T_1 and T_2 relaxation rates by restricting rotational motion. Proteins contain multiple functional groups which can interact with water through mechanisms that can affect relaxation, such as chemical exchange [15]. Additionally, a large portion of biofilms consist of cells, which represent another fraction of water with characteristic relaxation behavior [23]. While relaxation-weighted MRI cannot independently verify individual EPS molecules or all of the details of the EPS, better understanding of differences in NMR signal intensity and relaxation behavior will make this tool more effective for complementing more specific imaging techniques and helping combat the “identity crisis” of biofilm EPS.

2. Approach

2.1. Aerobic granular sludge (AGS) biofilm models

NMR is well suited to study biofilms in situ, though practical considerations are needed when establishing a system capable of growing a biofilm and integrating it into the spectrometer. Some biofilms are more amenable for NMR analysis than others. Aerobic granular sludge (AGS) are large (>200 μm), spherical biofilm aggregates formed from flocs of activated sludge for wastewater treatment [22]. They are of high technological interest and fit into standard NMR test tubes. To explore the influence that EPS components have on MRI contrast of AGS, artificial biofilm granule models are created using model representatives of different EPS components. Relaxation-weighted MRI of these model biofilms can then be compared to MRI of AGS granules. The subsequent sections will elaborate more on the roles of polysaccharides (PS), proteins (PN), and bacterial cells in AGS, and the criteria for selecting model representatives for the artificial biofilms.

2.2. Polysaccharides

Generally, the role of polysaccharides in the EPS is to provide structure and mechanical stability for the biofilm consortium. In AGS, the "structural EPS" is thought to mostly consist of polymers that cross-link together to form a hydrogel [2,3], which protects bacterial cells and encapsulates proteins, lipids, and other extracellular substances. Due to the high complexity of the composition of the EPS, not every polysaccharide has been identified, nor do all polysaccharides play a role in hydrogel formation [1]. To date, only two gel-forming extracellular polysaccharides have been isolated from AGS: alginate-like exopolysaccharide (ALE) (trade name Kaumera Nereda® Gum) and Granulan [24]. While hydrogels can be temperature or pH-induced [25], these polysaccharides form gels exclusively through ionic interactions.

2.3. Alginate-like exopolysaccharide (ALE)

Bacterial alginate was first isolated in 1966 and is produced by a wide range of Pseudomonas and Azotobacter species [26,27]. They are widely considered to be an important component in Pseudomonas biofilms [28]. Alginate-like exopolysaccharide (ALE) was isolated from AGS granules in 2010 [29]. The biomass was extracted using sodium carbonate and heat; ALE precipitated out of the supernatant by decreasing the pH with HCl. It is no surprise that the exopolysaccharide identified was "alginate-like" as these are the same steps used to isolate alginate from algae [29]. Both bacterial and plant-based alginates consist of two monomers, β-mannuronic (M) and α-glucuronic (G) acid, linked by 1–4 glycosidic bonds and carry a net negative charge due the presence of carboxylic acid functional groups. The monomers can be arranged into hetero- or homopolymeric "blocks" within the biopolymer (*i.e.,* MM, MG, and GG residues). According to the "egg-box" model for gelation, GG blocks form cavities which carry a −2 charge that fit/bind to divalent cations, particularly calcium, bringing biopolymer chains together to form a hydrogel [58]. Although plant-based alginate is distinguishable from bacterial alginate by the absence of o-acetyl groups on the monomers [29,30], it has been recognized as an excellent model for ALE [31] and was used as a model biopolymer in this study.

2.4. Granulan

Granulan was isolated by Seviour et al. [32] from lab-scale granules treating abattoir wastewater. Like ALE, the biomass was extracted under alkaline conditions, using NaOH instead of sodium carbonate, and Granulan precipitated out of the supernatant with cetylpyridinium chloride and methanol. Granulan is a complex heteropolysaccharide made up of repeating sequences of α-galactose, β-mannose, β-glucosamine, *N*-acetyl-β-galactosamine, and 2-acetoamido-2-deoxy-α-gal-actopyranuronic acid with an attached disaccharide branch of β-galactose and β-glucuronic acid. It is not known exactly which microbe synthesizes Granulan. Indeed, it might not be unique to any bacterial species, however, it has generally been found in reactors operating under conditions that enrich *Candidatus* "Competibacter phosphatis" bacteria. A gel is formed when strands of Granulan form anti-parallel, double helices stabilized by hydrogen bonding; the gel is strengthened when helices are connected by "interhelical bridges" formed by electrostatic interactions between divalent cations (calcium) and terminal carboxyl groups on β-Gal−β-GlcA residues. Because of the complexity of Granulan and its murky origins, it is difficult to isolate and study. However, there are many parallels between Granulan and gellan, an exopolysaccharide produced by pseudomonas elodea consisting of four polysaccharide units: two D-glucose, one D-glucuronic acid, and one L-rhamnose residue(s) [33]. Although comparatively much simpler, gellan has a similar gelling mechanism as Granulan. After the application of heat followed by slow cooling, gellan strands form anti-parallel, double helical structures stabilized by hydrogen bonds [34]. A stronger gel is generated when divalent cations are introduced, creating interhelical bridges between terminal carboxyl groups on glucuronic residues that link the helices together. In this study, gellan served as a model for Granulan.

2.5. Extracellular proteins

Extracellular proteins are the most abundant granule component [24]. Some researchers have found a strong correlation between the ratio of proteins to polysaccharides (PN/PS) and granule hydrophobicity, suggesting that proteins play an important role imparting hydrophobic properties which promote granulation [35]. Furthermore, proteins may help reduce the negative surface charge density surrounding bacterial cells, minimizing cell-cell repulsion [35]. In actual granules, PN/PS has been reported between 1 and 8, with larger values often observed during granulation [24]. The molecular weight (MW) of proteins in granular sludge has been reported to be 20–97 kDa [36]. Bovine serum albumin (BSA), a well-characterized protein standard consisting of 583 amino acid residues and MW of 66.5 kDa, was chosen to model extracellular proteins in the artificial biofilms.

2.6. Microorganisms

There can be no biofilm without bacterial cells, so it is no surprise that they represent a very large percentage (±15% by volume) of a hydrated biofilm [37]. Microbial populations in AGS are diverse, encompassing various bacterial and, in some cases, fungal species that vary based on substrate composition and growth environments [38]. While filamentous microorganisms can be present in AGS, floc-forming bacterial cells are typically the dominant component in stable AGS granules [39] and are the focus of this study.

With respect to NMR, cells are considered a highly restricted water population trapped inside a semipermeable membrane [9,23]. It is therefore not necessary to closely model any specific microorganism. *Bacillus mojavensis*, a gram-positive, aerobic rod-shape bacterium, was chosen to represent bacterial cells in the artificial biofilms.

3. Materials and methods

3.1. Alginate sample preparation

Medium viscosity sodium alginate (Sigma Aldrich) derived from brown seaweed was dissolved at concentrations ranging from 1 to 3% w/w in 0.1 M NaCl (Sigma Aldrich) solution prepared in deionized (DI) water. To incorporate protein into the alginate, lyophilized bovine serum albumin (BSA fraction V, fatty acid free; Caisson Labs) was added to alginate solution and allowed to fully disperse for several hours at 4 °C. The final concentration of alginate was fixed at 2% w/w while BSA ranged between 2 and 4% w/w. For cells immobilized in alginate, *B. mojavensis* culture was first spun down, supernatant removed, and the volume recorded (cell culture procedure outlined in section 3.5). Alginate solution prepared in 0.85% NaCl and 10 mM HEPES buffer was added to the pellet and mixed gently. Alginate was not supplemented with any nutrients to maintain metabolic activity during encapsulation. The final concentration of alginate was fixed at 2% w/w and cell concentrations were prepared at 10% and 20% v/v.

3.2. Alginate gelation procedure

Alginate solutions were carefully loaded into a 60 mL syringe to prevent bubble formation. The syringe was fitted with an 18G needle and then loaded onto a syringe pump. Alginate was added dropwise at 1 mL/min into a 0.5 M solution of $CaCl_2$ (Acros Organics) prepared in DI water at room temperature. Gel beads formed instantly and were allowed to mix with a magnetic stir bar at low speed for 1 h before removing for storage or NMR analysis.

The gelation agent for alginate/BSA mixtures was modified in order

to create a chitosan-alginate membrane around the bead to mitigate protein loss, adapted from a procedure by Takka et al. [40]. Chitosan was dissolved in 5% acetic acid at a concentration of 0.25% w/v. Next, 0.5 M $CaCl_2$ was prepared in this solution and the pH was adjusted to 5 with 0.1 M NaOH. Protein encapsulated alginate beads were formed in this media following the general procedure described above.

The gelation agent for alginate/cell mixtures was also changed to 0.2 M $CaCl_2$ prepared in 0.85% saline and 10 mM HEPES buffer. This media was also sterilized by autoclave (120°C for 20 min).

3.3. Gellan and gellan/alginate sample preparation and gelation procedure

Gellan gum powder (MP) was mixed into DI water at concentrations ranging from 1 to 3%. The solution was heated to 90°C until fully dissolved, then cooled to 45–55°C and loaded into a syringe. Gellan beads were formed in 0.2 M $CaCl_2$ and were allowed to mix with a magnetic stir bar at low speed for 1 h before removing for storage or NMR analysis. For alginate/gellan beads, alginate and gellan were combined in DI water with additional time allowed for alginate dissolution before following the same procedure as with plain gellan. Beads were prepared with varying amounts of alginate and gellan, but keeping the total amount of polysaccharide fixed at 2% w/w.

3.4. Encapsulation efficiency

Protein encapsulation efficiency was calculated using the Qubit™ protein assay (Thermo Fisher Scientific). BSA was extracted from the chitosan-alginate beads by breaking down the crosslinked biopolymer in 0.5% w/v sodium carbonate solution heated to 80°C; full details of the procedure can be found in Felz et al. [25]. Encapsulation efficiencies >90% were measured from the alginate/BSA beads.

3.5. B. Mojavensis cell culture

One mL cryovial of *B. mojavensis* culture was thawed and added to 100 mL of modified Brain-Heart Infusion (BHI) broth (36 g/L Brain Heart Infusion (BHI) [Becton, Dickinson and Co., Sparks, MD], 3 g/L $NaNO_3$, 0.75 g/L NH_4Cl, 40 g/L NaCl) inside a 250 mL flask at room temperature. After 24 h, 1 mL was transferred to fresh 100 mL of growth media. After 16 h of culturing, cells were harvested for alginate encapsulation.

3.6. Aerobic granular sludge

Samples of aerobic granular sludge (AGS) were collected from full-scale Nereda® sequencing batch reactors treating municipal wastewater in Utrecht (PNU reactor) and Vroomshoop, the Netherlands. Utrecht granules were imaged four days after sampling, while Vroomshoop granules were imaged approximately one month after sampling. A full description of the AGS granules can be found in Kirkland et al. [22].

3.7. Magnetic resonance imaging (MRI)

Relaxation-weighted images of the model biofilms were acquired using the ParaVision 6.0.1 Multi-Slice-Multi-Echo (MSME) pulse sequence on a 7.05 T (300 MHz) Bruker Avance III superconducting magnet. In this method, an initial 90-degree RF-pulse excites the spins, which is followed by a 180-degree RF pulse that refocuses the spins, forming a spin echo at the echo time (T_E). This MR signal is repeatedly refocused by applying a series of 180-degree RF pulses, generating a train of spin echoes at different echo times. This process occurs during a single acquisition of the pulse sequence. Slice selection gradients, applied during the RF pulses, selectively excite a slice in the sample. Read- and phase-encoding gradients are applied to map out spin-echo signal in **k**-space, a reciprocal domain which describes MR signal in terms of the applied magnetic field gradient and the duration for which the gradient is applied [11]. With each repeat of the experiment, set by the repetition time (T_R), a different line in k-space is collected. The Fourier Transform of $M \times N$ **k**-space data points produce an $M \times N$ pixel image.

The MSME sequence generates an image at each T_E with a set experimental repetition time, T_R, and slice position. This allows the T_2 relaxation time to be calculated at each voxel by fitting the exponential decay with a least-squares fitting, resulting in a map of T_2 relaxation times. T_2 maps are highlighted in this study, as they allow a more quantitative interpretation of MRI contrast, and were analyzed using Prospa v3.24 (Magritek Ltd, Wellington, NZ). However, spins diffusing in magnetic field gradients enhance signal attenuation, therefore, the calculated T_2 times are qualified as "effective" relaxation times that are specific to the magnetic field strength and imaging parameters ($T_{2,eff}$) [41,11].

T_1-weighted MRI provides images of the biofilm in which the pixel intensity depends on the T_R of the experiment and the T_1 of the material. Although more qualitative, they are useful for highlighting different biofilm features and have fast acquisition times. T_1 contrast is introduced by running MSME experiments with short T_R and T_E times. Only components in which $T_1 < T_R$ will fully recover their magnetization, and thus appear brighter in the image [11]. Short T_E times favor T_1-weighting by minimizing transverse relaxation before refocusing the spin echo.

Images of Vroomshoop AGS granules were acquired on a Bruker Avance III system with a 5.9 T (250 MHz) superconducting magnet. Images of Utrecht AGS granules were acquired on a 22.3 T (950 MHz) superconducting magnet using an Avance III HD console. A full description of the hardware used to image AGS granules can be found in Kirkland et al. [22]. A summary of the MRI parameters used in all experiments are shown in Table 1.

4. Results and discussion

4.1. MRI analysis of alginate

Cross-sectional $T_{2,eff}$ maps of alginate showed contrast between the model biofilm and bulk water (Fig. 1). The associated histogram revealed two distinct peaks, with signal from free water and the gel corresponding to the distribution with longer and shorter relaxation times, respectively (Fig. 2). As the concentration of alginate increased from 1 to 2 to 3% w/w, the $T_{2,eff}$ of the gel reduced from 27.5 to 24.1 to 21.4 ms, respectively, while the $T_{2,eff}$ mode of free water remained fixed around 42 ms (Table 2).

Alginate gels are known to have strong T_2-weighted MRI contrast [42]. The crosslinked biopolymer creates small pores that slow translational and rotational motion of water protons, enhancing relaxation [42]. Relaxation can also be interpreted in terms of "bound water", which refers to water protons trapped in restricted environments and associated with biomolecules in a solvation process. Relaxation can be caused by protons on molecules moving between free and bound water states by diffusion. Additionally, relaxation can be caused by chemical exchange between water protons and labile protons on specific polysaccharide functional groups, *i.e.*, hydroxyl protons on alginate monomers [15,43]. While these relaxation mechanisms are not mutually exclusive, B.P. Hills argued that chemical exchange dominates over all others in dilute polysaccharide systems [15]. This explains why T_1 relaxation times of alginate are typically reported similar to water, since this mechanism does not contribute strongly to T_1 relaxation. However, it strongly affects T_2 relaxation, and correctly predicts the T_2 correlation with alginate concentration observed in this study and others [44]. This indicates that T_2-weighted imaging can provide an assessment of alginate-like exopolysaccharide (ALE) concentrations in aerobic granular sludge (AGS) [22]. This work evaluates to what extent MRI contrast is imparted by other biofilm components such as proteins and cells.

Table 1
NMR Experiment parameters. Model biofilm measurements were made at 7.05 T (300 MHz), Vroomshoop AGS granule measurements at 5.9 T (250 MHz), and Utrecht AGS granule measurements at 22.3 T (950 MHz).

Parameter	Model Biofilm Measurements		Vroomshoop AGS Granule Measurements		Utrecht AGS Granule Measurements	
	T_1-Weighted	T_2-Weighted (Map)	T_1-Weighted	T_2-Weighted (Map)	T_1-Weighted	T_2-Weighted (Map)
Repetition time T_R (s)	0.55	5	0.6	5	0.55	5
Echo time T_E (ms)	8	8	5.6	5.6	5.3	5.3
Number of echoes	12	12	8	8	16	32
Number of averages	25	6	32	32	8	4
Image pixel resolution	128 × 128	128 × 128	128 × 128	128 × 128	128 × 128	128 × 128
Pixel resolution (μm)	39	39	39	39	47	47
Slice thickness (mm)	0.3	0.3	0.5	0.5	0.1	0.1
Measurement time	29 min 20 s	1 h 4 min	40 min 57 s	5 h 41 min	9 min 23 s	42 min

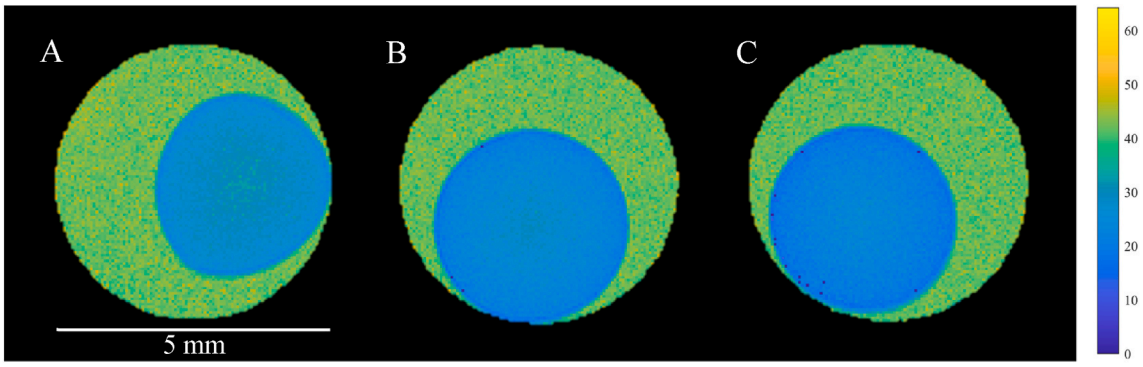

Fig. 1. Cross-sectional $T_{2,eff}$ maps of alginate model biofilms with increasing concentration of polysaccharide (1, 2 and 3% from A-C, respectively). The calculated $T_{2,eff}$ times are color-coded, with the shorter relaxation times, corresponding to the gel phase, in blue and longer relaxation times, corresponding to bulk water outside the gel, in yellow/green. Alginate concentration is strongly correlated with T_2 relaxation in the gel phase but does not influence bulk water relaxation. (For interpretation of the references to color in this figure legend, the reader is referred to the Web version of this article.)

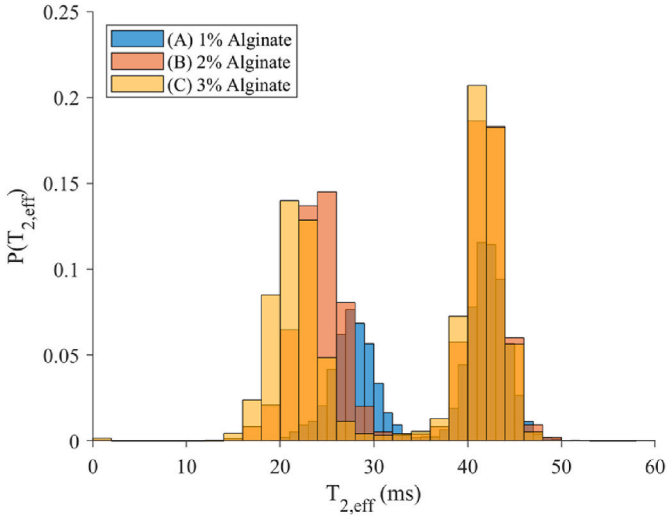

Fig. 2. $T_{2,eff}$ distribution profile of alginate model biofilms from Fig. 1.

The reported concentration of ALE in AGS varies in different studies but is a dominant exopolysaccharide. Lin et al. reported a yield of 160 mg crude EPS/g VSS (volatile suspended solids, *i.e.* dry biomass), or 16% w/w (dry) from Nereda® granules [29]. In lab-scale granules fed acetate as a carbon source, the yield was 31% w/w [45]. Taking the largest reported concentration, and given AGS is typically 95% water, it can be estimated that a mature granule contains up to 1.5% w/w bacterial alginate. Using a different approach, Seviour et al. [46] estimated a similar concentration of 1.22% w/w by correlating rheological behavior of granules to the gel-forming polysaccharide concentration and assuming only gel-forming components contributed to the granule modulus. In this study, 2% w/w alginate concentration was chosen as the baseline to model AGS biofilms.

It is acknowledged that there are obvious limitations with comparing carefully controlled alginate beads with organically formed AGS granules, which are heterogeneous and contain regions with high and low concentration of crosslinked biopolymer. However, the model biofilms are also not homogeneous, albeit in a predictable way. This can be observed visually in the MRI images as well as the $T_{2,eff}$ distribution profiles, in which there is a fairly large spread of relaxation times associated with the hydrogel (Fig. 2). Note this does not change with changing biopolymer concentration, as each profile maintains the same range and relative distribution. The heterogeneity in these biofilm models reflects the external gelation mechanism that alginate undergoes during preparation [47]. As calcium diffuses inside the alginate droplet, un-gelled alginate in the center diffuses towards the inwardly moving gel front, resulting in more densely crosslinked biopolymer from the outside-in. Nevertheless, these models demonstrate that alginate-like polymers provide strong T_2 relaxation-based contrast and MRI is sensitive to concentration differences across the sample.

Besides biopolymer concentration, the degree of crosslinking in alginate gels is also strongly dependent on the amount of GG residues. Several studies have shown that increased concentration of these blocks in alginate results in denser gels with enhanced T_1-and T_2-relaxation [42]. However, studies on monomer block concentrations in ALE reveal a complex situation. Initial reports showed that ALE has an unusually high amount of GG blocks (69.07%) compared to the MG fraction (14.57%) and MM fraction (2.10%) [29]. However, another study showed that during granule development, the fraction of MM blocks always stays low, the GG and MG fractions interchangeably dominate [48]. This adds yet another layer of complexity that must be considered if using MRI tools to characterize ALE concentration in AGS.

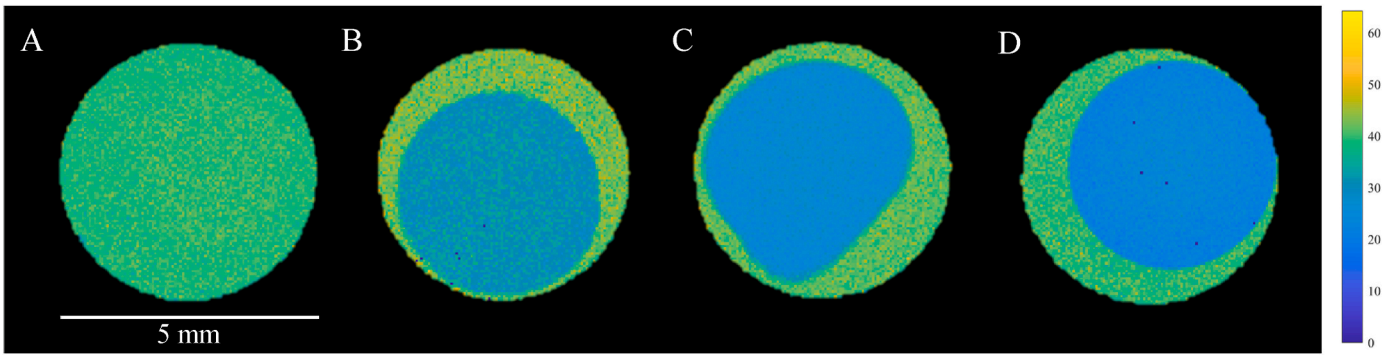

Fig. 3. $T_{2,eff}$ maps of mixed polysaccharide model biofilms consisting of gellan (G) and alginate (A) (2% gellan, G/A = 3, G/A = 1, G/A = 1/3, and from A-D, respectively). Total biopolymer concentration is fixed at 2% w/w in all samples. From A-D, as the concentration of gellan decreases, there is more T_2 contrast. The images highlight the sensitivity of MRI to alginate concentrations in mixed gels.

Table 2
$T_{2,eff}$ statistics (ms) of alginate model biofilms from Fig. 2.

Sample	Gel		Water	
	Mean	SD	Mean	SD
(A) 1% Alginate	27.5	2.3	42	1.9
(B) 2% Alginate	24.1	2.5	42	1.7
(C) 3% Alginate	21.4	2.6	41.8	1.7

4.2. MRI analysis of gellan

Gellan models showed negligible T_1-or T_2-weighted MRI contrast at concentrations ranging from 1 to 3% w/w, suggesting the T_1 and T_2 times of water inside the gel are very similar to bulk water ($T_{2,eff}$ map of 2% concentration shown in Fig. 3, A). This implies there are fewer labile protons undergoing chemical exchange in these gels. Like alginate, when gellan is ionically crosslinked, there is a reduction in the total number of exchangeable protons. However, hydrogen bonding is also essential in the gelation of gellan, facilitating the formation and stabilization of double helices and the three-dimensional gel network [34]. This interaction can significantly limit the number of functional groups which can undergo chemical exchange, a factor which has also been recognized in gelatine gels [15]. Fast diffusive exchange between water protons and bound water and/or fast chemical exchange between water protons and available labile protons on gellan –OH groups may also make relaxation times indistinguishable between the different proton fractions, resulting in minimal MRI contrast.

The reported concentration of Granulan has been reported as high as 320 mg crude EPS/g VSS, or 32% w/w (dry), a similar yield to ALE, although with further purification drops as low as 3% w/w [33]. Again, using the highest reported yield and the same assumption as before, a granule with Granulan as the major gel-forming component may contain up to 1.5% w/w of this exopolysaccharide. Because of the gelling process, granulation depends strongly on the quantity of Granulan present. This contrasts with ALE, in which granulation also depends on how M and G monomers are arranged. Provided gellan is a suitable model for Granulan, at its standard concentration, it appears very unlikely to provide much relaxation-weighted contrast, which serves as its own unique signature. Other biofilm components which show stronger MRI contrast have potential to be highlighted in these granules.

To explore the impacts of multiple gel-forming polysaccharides in one biofilm, experiments were conducted combining alginate with gellan at varying concentrations (Fig. 3, B-D, Fig. 4 and Table 3). Greater relaxation-weighted MRI contrast was found with higher amounts of alginate, again indicating the sensitivity of MRI to alginate concentration. However, the authors are not aware of any reports of ALE and Granulan being isolated from the same granule. Rather, it appears that either one or the other dominates depending on reactor conditions and

Table 3
$T_{2,eff}$ statistics (ms) of mixed polysaccharide model biofilms from Fig. 4.

Sample	Gel		Water	
	Mean	SD	Mean	SD
(A) 2% Gellan	39.1	1.7	39.1	1.7
(B) G/A = 3	31.1	2.2	42.7	2.4
(C) G/A = 1	25.9	1.7	41.4	1.9
(D) G/A = 1/3	23.3	1.9	39.7	2.2

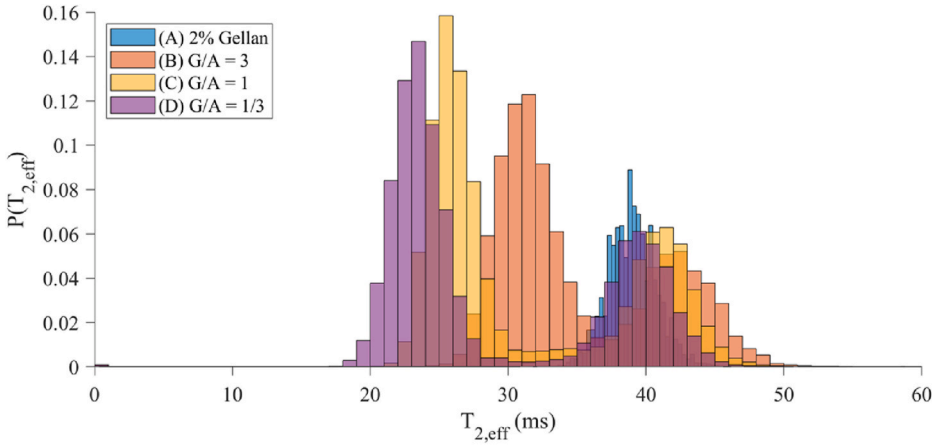

Fig. 4. $T_{2,eff}$ distribution profile of mixed polysaccharide model biofilms from Fig. 3.

which bacteria species are enriched [33]. Still, the unique relaxation-weighted MRI contrast shown by mixed polysaccharide model biofilms suggests that this tool holds promise in screening or characterizing biofilms that come from different backgrounds.

4.3. MRI analysis of bovine serum albumin (BSA) encapsulated in alginate

Adding BSA to 2% alginate resulted in reduced T_2 contrast (Fig. 5 and 6). The associated distribution profile shows two main peaks; as before, the distribution of longer and shorter relaxation times belongs to bulk water and the gel, respectively. Adding an equal amount of BSA and alginate biopolymer (PN/PS = 1) resulted in the average $T_{2,eff}$ of the gel increasing from 24.7 to 28.2 ms, while doubling the amount of protein (PN/PS = 2) increased the $T_{2,eff}$ to 32.2 ms (Table 4). Moreover, the gel becomes increasingly homogeneous after more protein is incorporated, with the $T_{2,eff}$ times becoming more concentrated around the mean in the distribution profiles.

As with polysaccharides, the origins of relaxation for proteins can also be explained with the "bound water" relaxation mechanism. Due to their size, protein macromolecules have long rotational mobility correlation times, *i.e.* slower rotational diffusion motion. This slows the motion of water associated with the protein as well, leading to enhanced T_1 and T_2 relaxation. Chemical exchange relaxation also occurs in proteins, which contain –NH, amides, –OH and –SH exchangeable groups from various amino acid moieties [15]. It is widely accepted that this mechanism plays the major role in enhancing relaxation in protein gels and solutions [49]. Consequently, the high concentration of BSA in the model biofilms was also expected to enhance T_2. However, the opposite trend was observed, suggesting there is a high degree of intermolecular actions, such as hydrogen bonding and ionic interactions, in the alginate-BSA gel which limits the number of labile protons available for chemical exchange with water protons.

An increase in the ionic strength of alginate solution can lead to the formation of more homogeneous and less rigid gel beads [50,51]. Ionic species introduce competition for the calcium ions for alginate GG blocks and ultimately limit the degree of Ca^{2+} crosslinking [50]. Under the gelation conditions of this study (pH 5), BSA is inside the range of its isoelectric point, but will contain positively charged amino acid residues. Since alginate is negatively charged, electrostatic interactions between the polysaccharide and protein can occur, which has been reported in several studies [52,53]. Although Zhao et al. [52] also reported that BSA-alginate ionic interactions are likely overtaken by Ca^{2+} during the gelation process, the concentration of BSA used in their study was 30-60x lower than the concentrations used here.

The complex protein and polysaccharide interactions on display in this study have parallels to those in actual granules. Polysaccharides and proteins in AGS can form crosslinks through permanent, covalent bonds as well as noncovalent interactions such as electrostatic, hydrophobic, and/or hydrogen bonds [54]. The extent of these protein-polysaccharide interactions has been revealed with enzymatic hydrolysis tests, which selectively target and break down polysaccharides or proteins. It was found that the removal of one component still led to the other component being reduced, demonstrating how well-integrated they are with each other [55]. This is also supported by CLSM images which show that proteins and polysaccharides are evenly distributed together throughout the granule [55]. The MRI studies show that protein-polysaccharide interactions influence relaxation-weighted images of model biofilms at a PN/PS of 1 and 2, even if proteins themselves do not impact relaxation directly. Interestingly, proteins were also shown to impact T_1 and T_2 MRI contrast minimally in brain tissue, which is composed of 8% protein, in a study which selectively cleared lipids from the tissue to see the contribution from proteins [56]. Future work should explore model biofilms with higher PN/PS ratios to further investigate how these interactions evolve and their impact on MRI relaxation behavior.

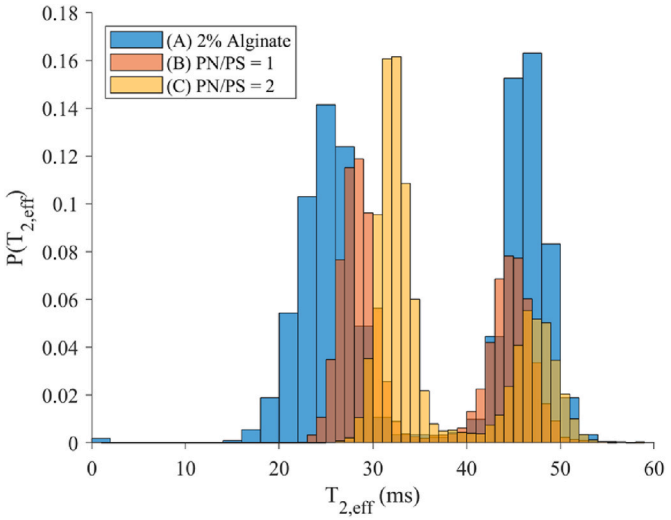

Fig. 6. $T_{2,eff}$ distribution profile of alginate/protein model biofilms from Fig. 5.

Table 4
$T_{2,eff}$ statistics (ms) of alginate/protein model biofilms from Fig. 6.

Sample	Gel		Water	
	Mean	SD	Mean	SD
(A) 2% Alginate	24.7	3.1	46.5	2.0
(B) PN/PS = 1	28.2	1.7	44.9	2.0
(C) PN/PS = 2	32.2	1.9	47.6	1.9

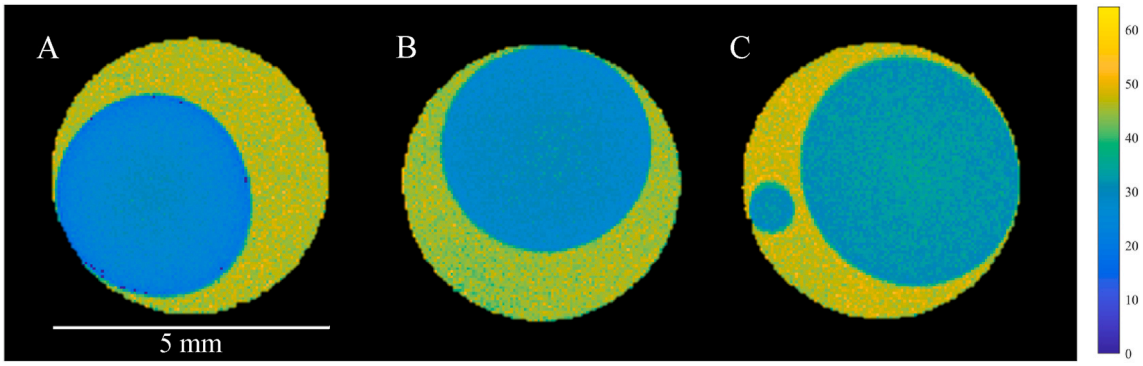

Fig. 5. $T_{2,eff}$ maps of alginate (PS, *i.e.* polysaccharide) model biofilms with increasing concentration of protein (PN) (2% alginate, PN/PS = 1, and PN/PS = 2 from A-C, respectively). Alginate concentration is fixed at 2% w/w in all samples. PN did not increase T_2 contrast as expected, instead, PS-PN interactions decreased T_2 MRI contrast.

4.4. MRI analysis of B. mojavensis encapsulated in alginate

Contrary to the previous biofilm models without bacteria, T_2 contrast was not observed at cell concentrations of 10 and 20% v/v with a fixed 2% w/w alginate concentration (Figs. 7 and 8 and Table 5). This was predicted by Kirkland et al. [22], who noted that cell surfaces have fewer labile protons available for chemical exchange compared to the surrounding EPS, or in the case of the model biofilms, the alginate.

However, MRI T_1 contrast was observed once cells were introduced. Fig. 7 (RHS) displays multiple echoes collected in a T_1-weighted experiment of 2% alginate with and without 20% v/v cells (Fig. 7, C–F and G-J, respectively). An echo time (T_E) of 8 ms was used in the first image and 3 T_E, 6 T_E, and 9 T_E were used in the subsequent images. In contrast to the $T_{2,eff}$ maps, which use a long repetition time (T_R) of 5 s, the T_1-weighted images use a much shorter T_R of 550 ms to highlight signal from short T_1 components, which recover their magnetization more quickly than long T_1 components. Plain alginate was undifferentiated from water in the first echo (Fig. 7, G), but showed clear contrast after cells were added (Fig. 7, C), generating a bimodal distribution of T_1-weighted signal intensities shown in Fig. 9. The bacteria contribute to higher intensity signal due to the lower T_1 from restricted water inside the cells (*i.e.*, intracellular water). With each progressive echo, the images become more T_2-weighted and the contrast starts to look similar, consistent with the results of the $T_{2,eff}$ maps.

Although T_1-weighted imaging introduced contrast from the cells, increasing the cell concentration from 10 to 20% did not enhance the T_1-weighted signal intensity significantly, with a mean increase of 3% (Fig. 9 and Table 6). The lack of enhancement was due to fixing the T_R time when running the imaging experiments. In principle, increasing the cell concentration will further lower T_1, albeit not to the same extent as from the no cell value. Nevertheless, fine tuning the T_R time could serve to optimize T_1 contrast at different cell concentrations. It should also be noted that in actual granules, bacteria reproduce and form clusters that exist in specific functional zones of the biofilm [38], exposing another limitation of using homogeneous biofilm models to study heterogeneous biofilms.

4.5. MRI analysis of wastewater reactor AGS granules

Insight from analyzing relaxation-weighted MRI contrast of model granules allows understanding of various regions of interest in environmental biofilms that are difficult to study, such as void spaces. Voids are one of the defining characteristics of all biofilms, generally described as water-filled regions composed of narrow, veiny channels and more voluminous, but not necessarily interconnected, pores. Gonzalez-Gil & Holliger [57] described the interior of AGS as "cavern-like", observing channels and cavities on the order of 10–100 μm using an invasive form of CLSM imaging. It has been hypothesized that pores arise in granules because of biomass decay due to substrate limited diffusion.

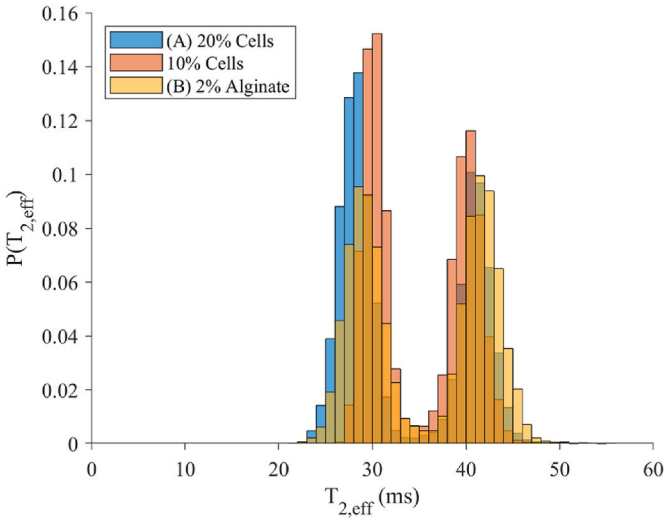

Fig. 8. $T_{2,eff}$ distribution profiles of alginate samples with and without cells from Fig. 7 (A-B). Image of 10% v/v cells encapsulated in alginate is not shown in Fig. 7, though included in this distribution profile.

Table 5
$T_{2,eff}$ statistics (ms) of alginate samples with and without cells from Fig. 8.

Sample	Gel		Water	
	Mean	SD	Mean	SD
2% Alginate	29	1.9	42	1.9
10% Cells	30	1.2	40	1.5
20% Cells	28	1.5	41	1.5

Consequently, pores may improve mass transport and lead to further biomass growth deeper within the biofilm. van den Berg [31] used less-invasive environmental scanning electron microscopy to study the microstructure of AGS harvested from a full-scale Nereda® wastewater plant, observing the presence of macropores (10–20 μm diameter) on the surface and interior of the granule. Other researchers have used relaxation-weighted MRI to visualize void regions in biofilm granules non-invasively. While channels were not explicitly observed, and may fall outside of the resolution limits of MRI, pores were visible [18,22]. Kirkland et al. [22] noted that relaxation times inside the pores fell within the range of free bulk water, as measured from quantitative $T_{2,eff}$ maps, indicating the pores were water-filled. However, the authors pointed out that dilute EPS components could still be present.

To analyze voids in wastewater biofilms, regions of interests (ROI) were drawn manually around voids from $T_{2,eff}$ maps and T_1-weighted MRI of AGS sampled from full scale WWT reactors (Figs. 10 and 13).

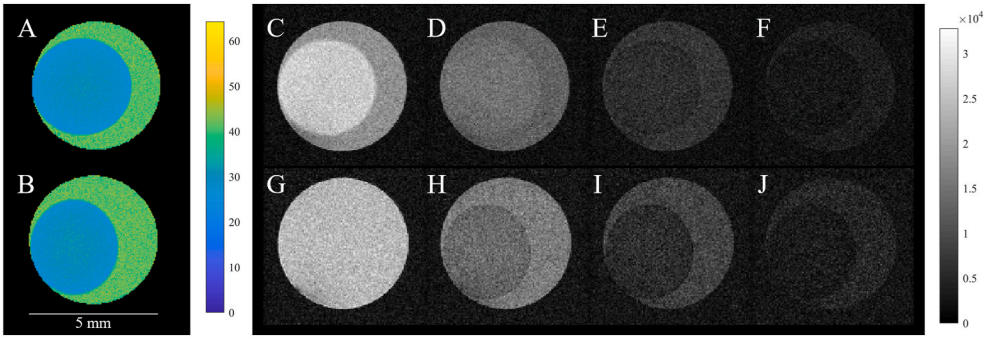

Fig. 7. LHS: $T_{2,eff}$ maps of alginate with and without 20% v/v cells (A and B, respectively). RHS: Corresponding T_1-weighted images of alginate samples with and without cells (C–F and G-J, respectively), with each image collected at different echo times, *i.e.* 8, 24, 48, and 72 ms from left to right. The addition of cells shows clear T_1 contrast, but $T_{2,eff}$ relaxation times are unaffected.

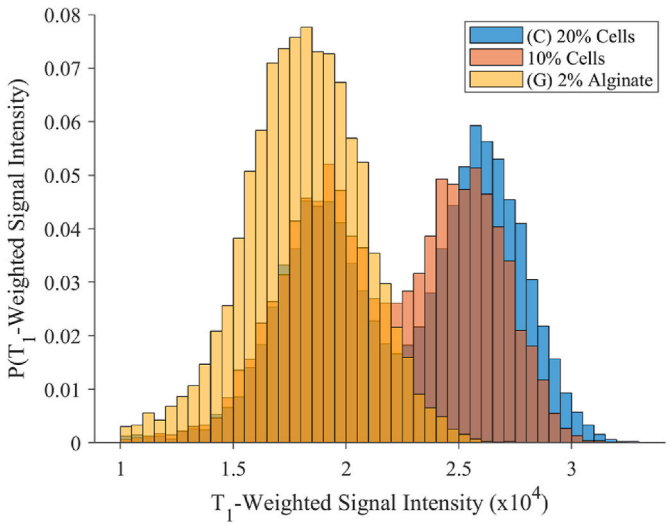

Fig. 9. T_1-weighted signal intensity distribution profiles of alginate samples with and without cells from Fig. 7 (C & G), taken from the first echo at 8 ms. Image of 10% v/v cells encapsulated in alginate is not shown in Fig. 7, though included in this distribution profile.

Table 6
T_1-weighted signal intensity statistics of alginate samples with and without cells from Fig. 9.

Sample	Gel		Water	
	Mean	SD	Mean	SD
2% Alginate	1.8×10^4	2.5×10^3	1.8×10^4	2.5×10^3
10% Cells	2.5×10^4	1.9×10^3	1.9×10^4	1.9×10^3
20% Cells	2.6×10^4	1.9×10^3	1.9×10^4	1.8×10^3

Since void regions are generally assumed to consist of free water, this signal was compared to free bulk water outside of the granule. This reference signal is important since these imaging experiments were conducted on different magnetic field strengths and with different imaging parameters compared to the experiments in this study (Table 1). Consequently, signal intensities and calculated $T_{2,eff}$ times are unique to each image. While this limits direct comparison to the model biofilms studied in this paper, it can be expected that the trends observed in the signal within the granule voids, compared to its reference free water signal, will align with the findings of this study. Additionally, by using spin-echo imaging and focusing on regions where signal is present, the impact of environmental components, such as minerals or solid inclusions, on relaxation behavior in the granules was assumed to be negligible.

The Vroomshoop granule contains a large void region and displays stronger T_2 (Figs. 10 (A) and 11 & Table 7) and T_1 (Figs. 10 (B) and 12 & Table 8) contrast in comparison to the bulk water signal, indicating distinct relaxation behavior within this void. The lower $T_{2,eff}$ times suggest dilute crosslinked biopolymer that may be alginate-like, while the stronger T_1 contrast indicates these regions may also contain cells. Although it is not possible to determine the exact source of these signals due to the non-specific nature of MRI contrast, these findings point to heterogeneity in the void composition and challenge the assumption that biofilm voids are either uniform or entirely empty. Higher protein concentrations could also be present due to the lower contrast in the crosslinked polysaccharide, but the relaxation behavior observed in the model biofilms limits precise characterization. It has been theorized that void regions form as granules starve aerobically, causing the EPS to break down and release cells from the biofilm so they can move to more

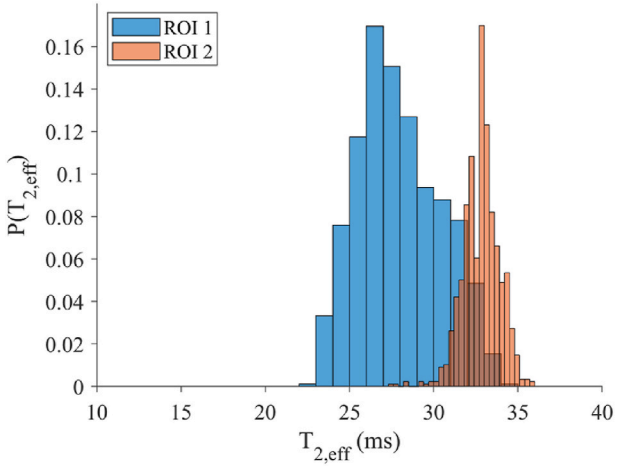

Fig. 11. $T_{2,eff}$ distribution profiles of Vroomshoop AGS granule from Fig. 10 (A), showing enhanced T_2 contrast inside the void (ROI 1). This relaxation behavior could be attributed to lightly crosslinked polymer.

Table 7
$T_{2,eff}$ statistics (ms) of Vroomshoop AGS granule from Fig. 11.

ROI	Mean	SD
1	27.9	2.5
2	32.9	1.0

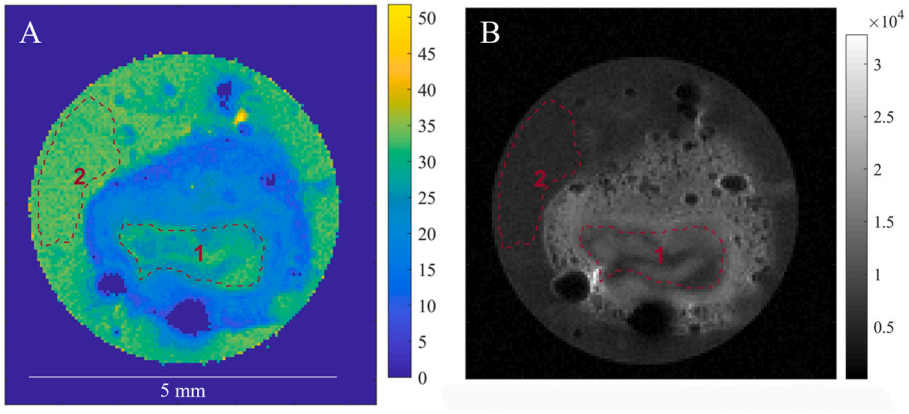

Fig. 10. LHS: $T_{2,eff}$ map of a full-scale Vroomshoop AGS granule. The regions of interest (ROI) compare a void space inside the granule (ROI 1) with bulk water outside of the granule (ROI 2). RHS: Corresponding T_1-weighted image showing the same ROI.

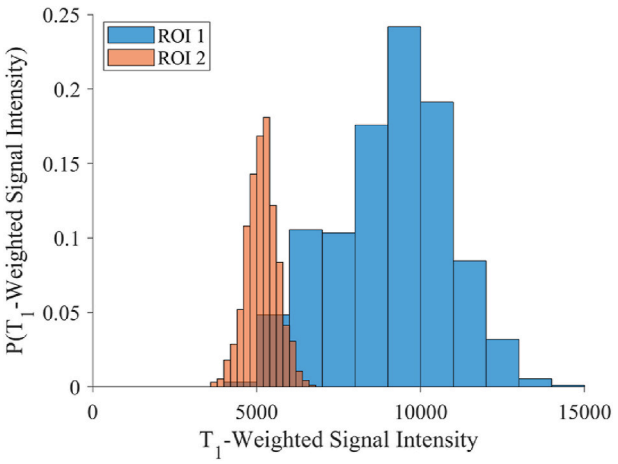

Fig. 12. T_1-weighted signal intensity distribution profiles of Vroomshoop AGS granule from Fig. 10 (B), showing enhanced T_1 contrast inside the void (ROI 1). This signature could be attributed to the presence of cells.

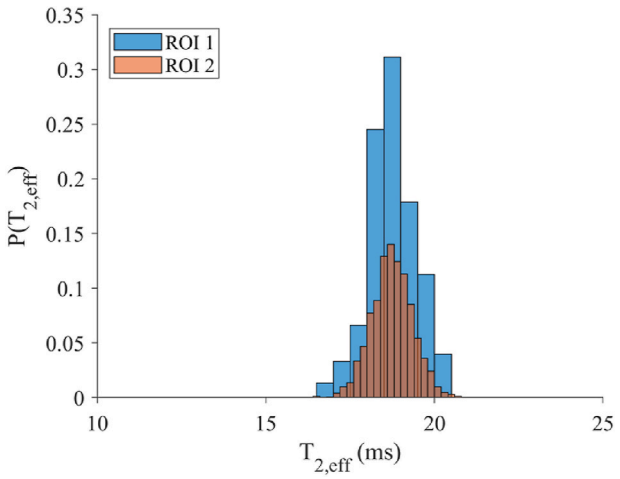

Fig. 14. $T_{2,eff}$ distribution profiles of Utrecht AGS granule from Fig. 13 (A), showing similar T_2 contrast between the void and bulk water (ROI 1 and 2, respectively). This relaxation behavior suggests the void is empty or contains very dilute polymer.

Table 8
T_1-weighted statistics of Vroomshoop AGS granule from Fig. 12.

ROI	Mean	SD
1	9.0×10^3	2×10^3
2	5.1×10^3	5×10^2

Table 9
$T_{2,eff}$ statistics (ms) of Utrecht AGS granule from Fig. 14.

ROI	Mean	SD
1	18.7	0.7
2	18.7	0.6

favorable conditions, a phenomenon which could explain the MRI contrast observed in this area. The void inside the Utrecht granule (Fig. 13, A) displays $T_{2,eff}$ times that align well with the bulk water relaxation times (Fig. 14 & Table 9). However, there is noticeably more T_1 contrast (+30%) in the T_1-weighted image (Figs. 13 (B) and 15 & Table 10). This may indicate cells present inside very dilute biopolymer. These findings raise new questions about the complexity of voids in biofilms, and future studies using higher-resolution techniques will be crucial to fully characterize these regions.

5. Conclusion

In this study, the use of non-invasive, relaxation-weighted MRI to characterize major biofilm and EPS components was explored using model biofilms of aerobic granular sludge (AGS). The main findings are:

- Certain gel-forming polysaccharides, such as alginate, a model for ALE, generate T_2 contrast while providing negligible T_1-weighted contrast. $T_{2,eff}$ times of alginate correlate with biopolymer concentration, allowing MRI to differentiate high- and low-density ALE regions.
- Other gel-forming polysaccharides, such as gellan, a model for Granulan, displayed no T_1 or T_2 contrast.
- BSA, a model for extracellular proteins, was found to increase T_2 relaxation times when combined with alginate at a PN/PS of 1 and 2. Mixtures of protein and polysaccharide affect relaxation behavior by forming complex interactions with each other that alter the degree of alginate crosslinking.
- Bacterial cells immobilized in alginate at concentrations of 10 and 20% v/v did not alter T_2 contrast but strongly enhanced T_1-weighted contrast. As cell clusters contained in biofilms may exist at even higher concentrations tested here, further studies are needed to determine if this trend holds.

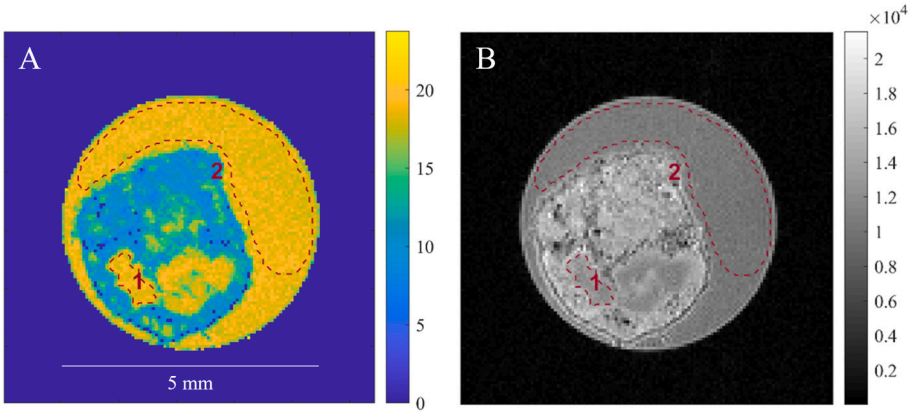

Fig. 13. LHS: $T_{2,eff}$ map of a full-scale Utrecht AGS granule. The regions of interest (ROI) compare a void space inside the granule (ROI 1) with bulk water outside of the granule (ROI 2). RHS: Corresponding T_1-weighted image showing the same ROI.

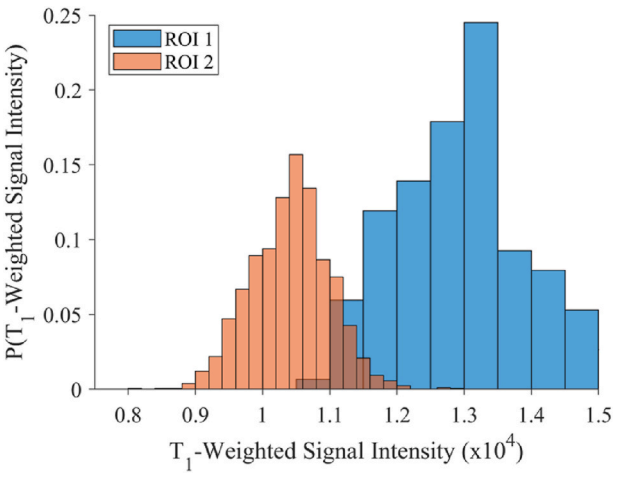

Fig. 15. T_1-weighted signal intensity distribution profiles of Utrecht AGS granule from Fig. 13 (B) showing enhanced T_1 contrast inside the void (ROI 1). This signature could be attributed to the presence of cells.

Table 10
T_1-weighted statistics of Utrecht AGS granule from Fig. 15.

ROI	Mean	SD
1	1.3×10^4	1×10^3
2	1.0×10^4	6×10^2

- Trends in the model biofilms were used as a baseline to explore T_2 and T_1-weighted contrast in void regions of two different AGS granules to qualitatively assess EPS components present.

Even in these simple biofilm models, complex NMR relaxation behavior was observed, underscoring the challenges in interpreting MRI signals from heterogeneous biofilms. As such, future work should explore the impact of other biofilm components, such as DNA and lipids, on relaxation behavior. Nevertheless, the findings show that relaxation-weighted MRI can offer a unique perspective by providing insights not only into biofilm heterogeneity, but also into the composition of biopolymers, cells, and water within these complex systems. This represents another step in leveraging this valuable experimental method to study biofilm EPS and identify areas for more detailed analysis.

CRediT authorship contribution statement

Matthew R. Willett: Writing – original draft, Visualization, Methodology, Investigation, Conceptualization. **Sarah L. Codd:** Writing – review & editing, Conceptualization. **Joseph D. Seymour:** Writing – review & editing, Methodology, Conceptualization. **Catherine M. Kirkland:** Writing – review & editing, Supervision, Resources, Methodology, Funding acquisition, Conceptualization.

Declaration of competing interest

The authors declare that they have no known competing financial interests or personal relationships that could have appeared to influence the work reported in this paper.

Acknowledgements

This research did not receive any specific grant from funding agencies in the public, commercial, or not-for-profit sectors. SLC was supported by the National Institute of General Medical Sciences of the National Institutes of Health under Award Number P20GM103474. The content is solely the responsibility of the authors and does not necessarily represent the official views of the National Institutes of Health. The authors thank Joelle Wolf and Madeline Pernat (Montana State University) for helping prepare model biofilm samples and Dr. Markus Dieser (Montana State University) for access to the Invitrogen Qubit™ Fluorometer used in this study.

Data availability

Data will be made available on request.

References

[1] Seviour T, Derlon N, Dueholm MS, Flemming HC, Girbal-Neuhauser E, Horn H, Kjelleberg S, van Loosdrecht MCM, Lotti T, Malpei MF, Nerenberg R, Neu TR, Paul E, Yu H, Lin Y. Extracellular polymeric substances of biofilms: suffering from an identity crisis. Water Res 2019;151:1–7. https://doi.org/10.1016/j.watres.2018.11.020.
[2] Sutherland IW. Biofilm exopolysaccharides : a strong and sticky framework. Microbiology (Society for General Microbiology) 2001;147(Pt 1):3–9. https://doi.org/10.1099/00221287-147-1-3.
[3] Flemming HC, Wingender J. The biofilm matrix. Nat Rev Microbiol 2010;8(9):623–33. https://doi.org/10.1038/nrmicro2415.
[4] Abreu AC, Fernández I. Nuclear magnetic resonance to study bacterial biofilms structure, formation, and resilience. In: Recent trends in biofilm science and technology; 2020. p. 23–70. https://doi.org/10.1016/b978-0-12-819497-3.00002-7.
[5] van Hoogstraten SWG, Kuik C, Arts JJC, Cillero-Pastor B. Molecular imaging of bacterial biofilms-a systematic review. Crit Rev Microbiol 2023:1–22. https://doi.org/10.1080/1040841X.2023.2223704.
[6] Callaghan PT. Principles of nuclear magnetic resonance microscopy. Oxford University Press; 1991.
[7] Blümich B. Essential NMR for scientists and engineers. Springer; 2005.
[8] Herrling MP, Lackner S, Nirschl H, Horn H, Guthausen G. Chapter Four - recent NMR/MRI studies of biofilm structures and dynamics. In: Webb GA, editor. Annual reports on NMR spectroscopy, vol. 97. Academic Press; 2019. p. 163–213. https://doi.org/10.1016/bs.arnmr.2019.02.001.
[9] Seymour JD, Codd SL, Gjersing EL, Stewart PS. Magnetic resonance microscopy of biofilm structure and impact on transport in a capillary bioreactor. J Magn Reson 2004;167(2). https://doi.org/10.1016/j.jmr.2004.01.009.
[10] Quan K, Hou J, Zhang Z, Ren Y, Peterson BW, Flemming HC, Mayer C, Busscher HJ, van der Mei HC. Water in bacterial biofilms: pores and channels, storage and transport functions. Crit Rev Microbiol 2022;48(3):283–302. https://doi.org/10.1080/1040841X.2021.1962802.
[11] Blümich B. NMR imaging of materials. 2000. Oxford.
[12] Majors PD, McLean JS, Pinchuk GE, Fredrickson JK, Gorby YA, Minard KR, Wind RA. NMR methods for in situ biofilm metabolism studies. J Microbiol Methods 2005;62(3):337–44. https://doi.org/10.1016/j.mimet.2005.04.017.
[13] Mitra M. Nuclear magnetic resonance (NMR) and surface plasmon resonance (SPR) imaging as an advanced tool for examining biofilm matrix (structure, composition, and dynamics). In: Moupriya Nag DL, editor. Analytical methodologies for biofilm research. Springer Protocol Handbooks; 2021. p. 243–68.
[14] Vogt SJ, Sanderlin AB, Seymour JD, Codd SL. Permeability of a growing biofilm in a porous media fluid flow analyzed by magnetic resonance displacement-relaxation correlations. Biotechnol Bioeng 2013;110(5):1366–75. https://doi.org/10.1002/bit.24803.
[15] Hills BP. The proton exchange cross-relaxation model of water relaxation in biopolymer systems. Mol Phys 1992;76(3):509–23. https://doi.org/10.1080/00268979200101501.
[16] Herrling MP, Weisbrodt J, Kirkland CM, Williamson NH, Lackner S, Codd SL, Seymour JD, Guthausen G, Horn H. NMR investigation of water diffusion in different biofilm structures. Biotechnol Bioeng 2017;114(12):2857–67. https://doi.org/10.1002/bit.26392.
[17] Wieland A, de Beer D, Damgaard LR, Kühl M, van Dusschoten D, Van As H. Fine-scale measurement of diffusivity in a microbial mat with nuclear magnetic resonance imaging. Limnol Oceanogr 2001;46(2):248–59. https://doi.org/10.4319/lo.2001.46.2.0248.
[18] Phoenix VR, Holmes WM. Magnetic resonance imaging of structure, diffusivity, and copper immobilization in a phototrophic biofilm. Appl Environ Microbiol 2008;74(15):4934–43. https://doi.org/10.1128/AEM.02783-07.
[19] Cimmarusti GM. *Magnetic resonance imaging Characterization of porous Substrates and Models of Soil and biofilms* [doctor of philosophy. University of Birmingham]; 2021.
[20] Sayers EW, Weaver JL, Prestegard JH. Hydrogen bonding geometry of a protein-bound carbohydrate from water exchange-mediated cross-relaxation. J Biomol NMR 1998;12(2):209–22. https://doi.org/10.1023/A:1008220522409.
[21] Hoskins BC, Majors P, Sharma MM, Georgiou G. Non-invasive imaging of biofilms in porous media using NMR methods. SPE/EPA exploration and production environmental conference. 1999. https://doi.org/10.2118/52733-MS.
[22] Kirkland CM, Krug JR, Vergeldt FJ, van den Berg L, Velders AH, Seymour JD, Codd SL, Van As H, de Kreuk MK. Characterizing the structure of aerobic granular sludge using ultra-high field magnetic resonance. Water Sci Technol 2020;82(4):627–39. https://doi.org/10.2166/wst.2020.341.

[23] Beuling EE, van Dusschoten D, Lens P, van den Heuvel JC, Van As H, Ottengraf SPP. Characterization of the diffusive properties of biofilms using pulsed field gradient-nuclear magnetic resonance. Biotechnol Bioeng 1998;60:283–91. https://doi.org/10.1002/(sici)1097-0290(19981105)60:3<283::aid-bit3>3.0.co;2-d.
[24] Cydzik-Kwiatkowska A. Biopolymers in aerobic granular sludge—their role in wastewater treatment and possibilities of Re-use in line with circular economy. Energies 2021;14(21). https://doi.org/10.3390/en14217219.
[25] Felz S, Al-Zuhairy S, Aarstad OA, van Loosdrecht MC, Lin YM. Extraction of structural extracellular polymeric substances from aerobic granular sludge. J Vis Exp 2016;115. https://doi.org/10.3791/54534.
[26] Linker A, Jones RS. A new polysaccharide resembling alginic acid isolated from pseudomonads. J Biol Chem 1966;241(16):3845–51. https://doi.org/10.1016/S0021-9258(18)99848-0.
[27] Gacesa P. Bacterial alginate biosynthesis - recent progress and future prospects. Microbiology 1998;144(5):1133–43. https://doi.org/10.1099/00221287-144-5-1133.
[28] Hay ID, Wang Y, Moradali MF, Rehman ZU, Rehm BHA. Genetics and regulation of bacterial alginate production. Environ Microbiol 2014;16(10):2997–3011. https://doi.org/10.1111/1462-2920.12389.
[29] Lin Y, de Kreuk M, van Loosdrecht MC, Adin A. Characterization of alginate-like exopolysaccharides isolated from aerobic granular sludge in pilot-plant. Water Res 2010;44(11):3355–64. https://doi.org/10.1016/j.watres.2010.03.019.
[30] Fabich HT, Vogt SJ, Sherick ML, Seymour JD, Brown JR, Franklin MJ, Codd SL. Microbial and algal alginate gelation characterized by magnetic resonance. J Biotechnol 2012;161(3). https://doi.org/10.1016/j.jbiotec.2012.04.016.
[31] van den Berg L, Toja Ortega S, van Loosdrecht MCM, de Kreuk MK. Diffusion of soluble organic substrates in aerobic granular sludge: effect of molecular weight. Water Res X 2022;16:100148. https://doi.org/10.1016/j.wroa.2022.100148.
[32] Seviour T, Donose BC, Pijuan M, Yuan Z. Purification and conformational analysis of a key exopolysaccharide component of mixed culture aerobic sludge granules. Environ Sci Technol 2010;44(12):4729–34. https://doi.org/10.1021/es100362b.
[33] Seviour T, Yuan Z, van Loosdrecht MC, Lin Y. Aerobic sludge granulation: a tale of two polysaccharides? Water Res 2012;46(15):4803–13. https://doi.org/10.1016/j.watres.2012.06.018.
[34] Bacelar AH, Silva-Correia J, Oliveira JM, Reis RL. Recent progress in gellan gum hydrogels provided by functionalization strategies. J Mater Chem B 2016;4(37):6164–74. https://doi.org/10.1039/c6tb01488g.
[35] Zhang L, Feng X, Zhu N, Chen J. Role of extracellular protein in the formation and stability of aerobic granules. Enzym Microb Technol 2007;41(5):551–7. https://doi.org/10.1016/j.enzmictec.2007.05.001.
[36] Zhu L, Zhou J, Lv M, Yu H, Zhao H, Xu X. Specific component comparison of extracellular polymeric substances (EPS) in flocs and granular sludge using EEM and SDS-PAGE. Chemosphere 2015;121:26–32. https://doi.org/10.1016/j.chemosphere.2014.10.053.
[37] Donlan R. Biofilms: microbial life on surfaces. Emerg Infect Dis 2002;8(9):881–90. https://doi.org/10.3201/eid0809.020063.
[38] Hou Y, Gan C, Chen R, Chen Y, Yuan S, Chen Y. Structural characteristics of aerobic granular sludge and factors that influence its stability: a mini review. Water 2021;13(19):2726. https://doi.org/10.3390/w13192726.
[39] Liu X, Li R, Chen R, Chen Y, Zeng A, Deng Y, Ma J, Chen M. Formation of filamentous fungal pellets in aerobic granular sludge via reducing temperature and dissolved oxygen: characteristics of filamentous fungi and denitrification performance. Bioresour Technol 2021;332:125056. https://doi.org/10.1016/j.biortech.2021.125056. 125056.
[40] Takka S, Gurel A. Evaluation of chitosan/alginate beads using experimental design: formulation and in vitro characterization. AAPS PharmSciTech 2010;11(1):460–6. https://doi.org/10.1208/s12249-010-9406-z.
[41] Edzes H, van Dusschoten D, Van As H. Quantitative T_2 imaging of plant tissues by means of multi-echo MRI microscopy. Magn Reson Imaging 1998;16(2):185–96. https://doi.org/10.1016/s0730-725x(97)00274-9.
[42] Simpson NE, Grant SC, Blackband SJ, Constantinidis I. NMR properties of alginate microbeads. Biomaterials 2003;24(27):4941–8. https://doi.org/10.1016/s0142-9612(03)00418-6.
[43] Hester-Reilly HJ, Shapley NC. Imaging contrast effects in alginate microbeads containing trapped emulsion droplets. J Magn Reson 2007;188(1):168–75. https://doi.org/10.1016/j.jmr.2007.05.022.
[44] Potter K, Carpenter TA, Hall L. Mapping of the spatial variation in alginate concentration in calcium alginate gels by magnetic resonance imaging (MRI). Carbohydr Res 1993;246(1):43–9. https://doi.org/10.1016/0008-6215(93)84022-X.
[45] Lin YM, Wang L, Chi ZM, Liu XY. Bacterial alginate role in aerobic granular bioparticles formation and settleability improvement. Separ Sci Technol 2008;43(7):1642–52. https://doi.org/10.1080/01496390801973805.
[46] Seviour T, Pijuan M, Nicholson T, Keller J, Yuan Z. Gel-forming exopolysaccharides explain basic differences between structures of aerobic sludge granules and floccular sludges. Water Res 2009;43(18):4469–78. https://doi.org/10.1016/j.watres.2009.07.018.
[47] Smidsrod O, Draget KL. Chemistry and physical properties of alginates. Carbohydr Eur J 1996;14:6–13.
[48] Yang YC, Liu X, Wan C, Sun S, Lee DJ. Accelerated aerobic granulation using alternating feed loadings: alginate-like exopolysaccharides. Bioresour Technol 2014;171:360–6. https://doi.org/10.1016/j.biortech.2014.08.092.
[49] Venu K, Denisov VP, Halle B. Water 1H magnetic relaxation dispersion in protein solutions. A quantitative assessment of internal hydration, proton exchange, and cross-relaxation. J Am Chem Soc 1997;119(13):3122–34. https://doi.org/10.1021/ja963611t.
[50] LeRoux MA, Guilak F, Setton LA. Compressive and shear properties of alginate gel: effects of sodium ions and alginate concentration. J Biomed Mater Res 1999;47(1):46–53. https://doi.org/10.1002/(SICI)1097-4636(199910)47:1<46::AID-JBM6>3.0.CO;2-N.
[51] Lee BB, Ravindra P, Chan ES. Size and shape of calcium alginate beads produced by extrusion dripping. Chem Eng Technol 2013;36(10):1627–42. https://doi.org/10.1002/ceat.201300230.
[52] Zhao Y, Li F, Carvajal MT, Harris MT. Interactions between bovine serum albumin and alginate: an evaluation of alginate as protein carrier. J Colloid Interface Sci 2009;332(2):345–53. https://doi.org/10.1016/j.jcis.2008.12.048.
[53] Zhang Y, Wang QC, Yu H, Zhu J, de Lange K, Yin Y, Wang Q, Gong J. Evaluation of alginate-whey protein microcapsules for intestinal delivery of lipophilic compounds in pigs. J Sci Food Agric 2016;96(8):2674–81. https://doi.org/10.1002/jsfa.7385.
[54] Li Z, Lin L, Liu X, Wan C, Lee DJ. Understanding the role of extracellular polymeric substances in the rheological properties of aerobic granular sludge. Sci Total Environ 2020;705:135948. https://doi.org/10.1016/j.scitotenv.2019.135948.
[55] Wang S, Huang X, Liu L, Yan P, Chen Y, Fang F, Guo J. Insight into the role of exopolysaccharide in determining the structural stability of aerobic granular sludge. J Environ Manag 2021;298:113521. https://doi.org/10.1016/j.jenvman.2021.113521.
[56] Leuze C, Aswendt M, Ferenczi E, Liu CW, Hsueh B, Goubran M, Tian Q, Steinberg G, Zeineh MM, Deisseroth K, McNab JA. The separate effects of lipids and proteins on brain MRI contrast revealed through tissue clearing. Neuroimage 2017;156:412–22. https://doi.org/10.1016/j.neuroimage.2017.04.021.
[57] Gonzalez-Gil G, Holliger C. Aerobic granules: microbial landscape and architecture, stages, and practical implications. Appl Environ Microbiol 2014;80(11):3433–41. https://doi.org/10.1128/AEM.00250-14.
[58] Grant GT, Morris ER, Rees DA, Smith PJC, Thom D. Biological interactions between polysaccharides and divalent cations: the egg-box model. FEBS Lett 1973;32(1):195–8. https://doi.org/10.1016/0014-5793(73)80770-7.